Electronic Supplementary Material (ESI) for Journal of Materials Chemistry A.

Supporting information

Titanium and fluorine synergetic modification improves the electrochemical performance of $Li(Ni_{0.8}Co_{0.1}Mn_{0.1})O_2$

Zheng Si, [a] Baozhao Shi, [a] Jin Huang, [b] Ye Yu, [b] You Han, [a] Jinli Zhang, [a,c] Wei Li *[a]

[a]*School of Chemical Engineering and Technology, Tianjin University, Tianjin 300350, P. R. China.*

[b] *Guizhou Zhenhua E-CHEM Co.,Ltd., Guiyang550014, P. R. China.*

[c] *School of Chemistry and Chemical Engineering, Shihezi University, Shihezi 832003, P. R. China.*

（Corresponding author: liwei@tju.edu.cn）

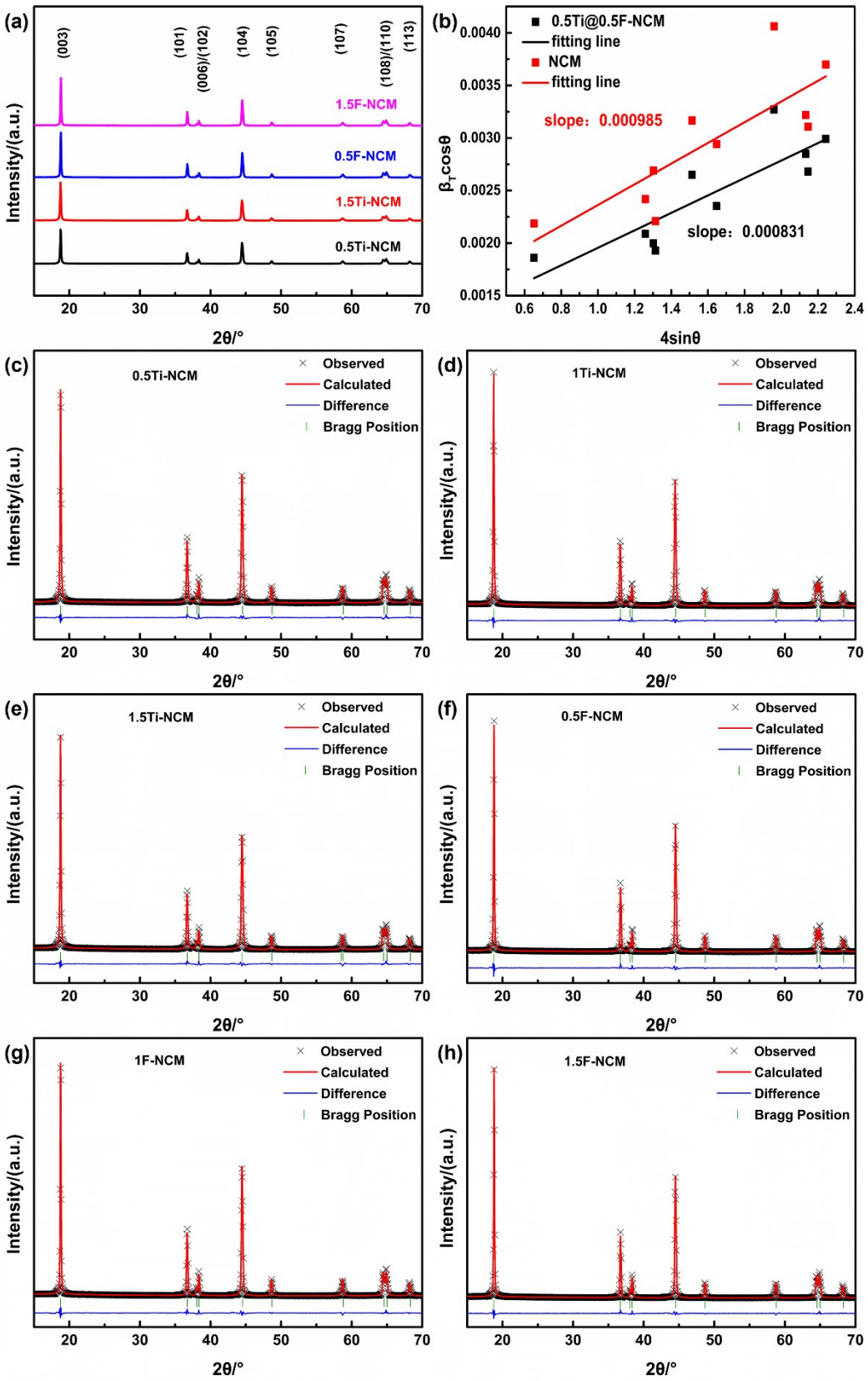

Figure S1. XRD patterns of 0.5Ti-NCM, 1.5Ti-NCM,0.5F-NCM, and 1.5F-NCM (a), Williamson-Hall plots of NCM and 0.5Ti@0.5F-NCM (b), Rietveld refinement of the XRD patterns for 0.5Ti-NCM, 1Ti-NCM, 1.5Ti-NCM, 0.5F-NCM, 1F-NCM and 1.5F-NCM (c-g).

Williamson-Hall plot method:

In XRD pattern, the broadening (β_T) of the peaks is due to the combine effect of crystallites size (β_D) and lattice strain (β_ε).

$$\beta_T = \beta_D + \beta_\varepsilon$$

$$\beta_T = \frac{K\lambda}{D\cos\theta} + 4\,\varepsilon\tan\theta$$

therefore,

$$\beta_T cos\theta = \varepsilon(4\sin\theta) + \frac{K\lambda}{D}$$

So, the slope of Williamson-Hall plot is the lattice strain for materials.

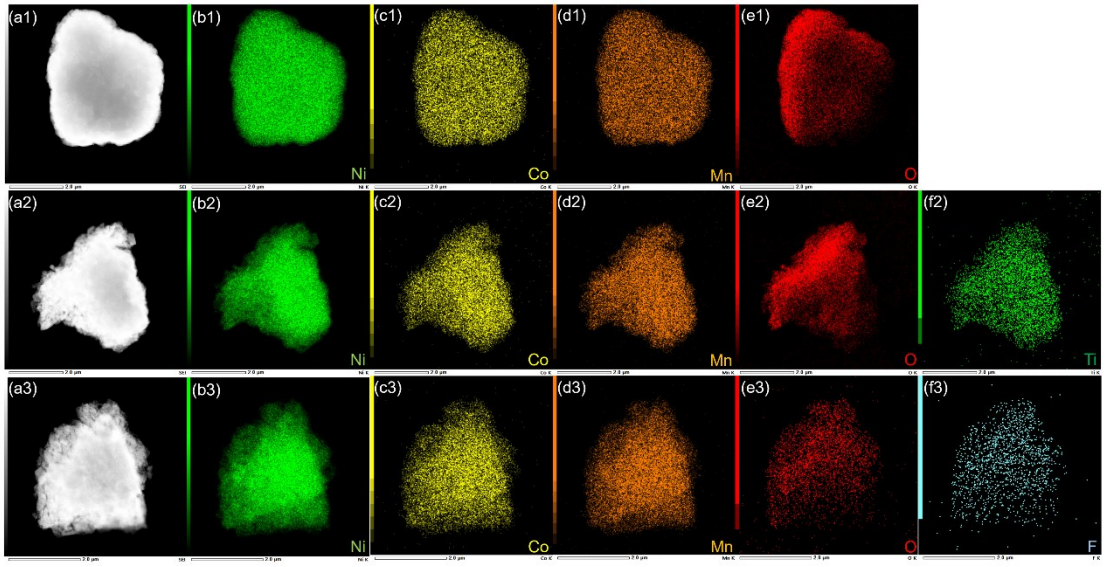

Figure S2. EDS mapping images of NCM (a1-e1), 1Ti-NCM(a2-f2) and 1F-NCM(a3-f3).

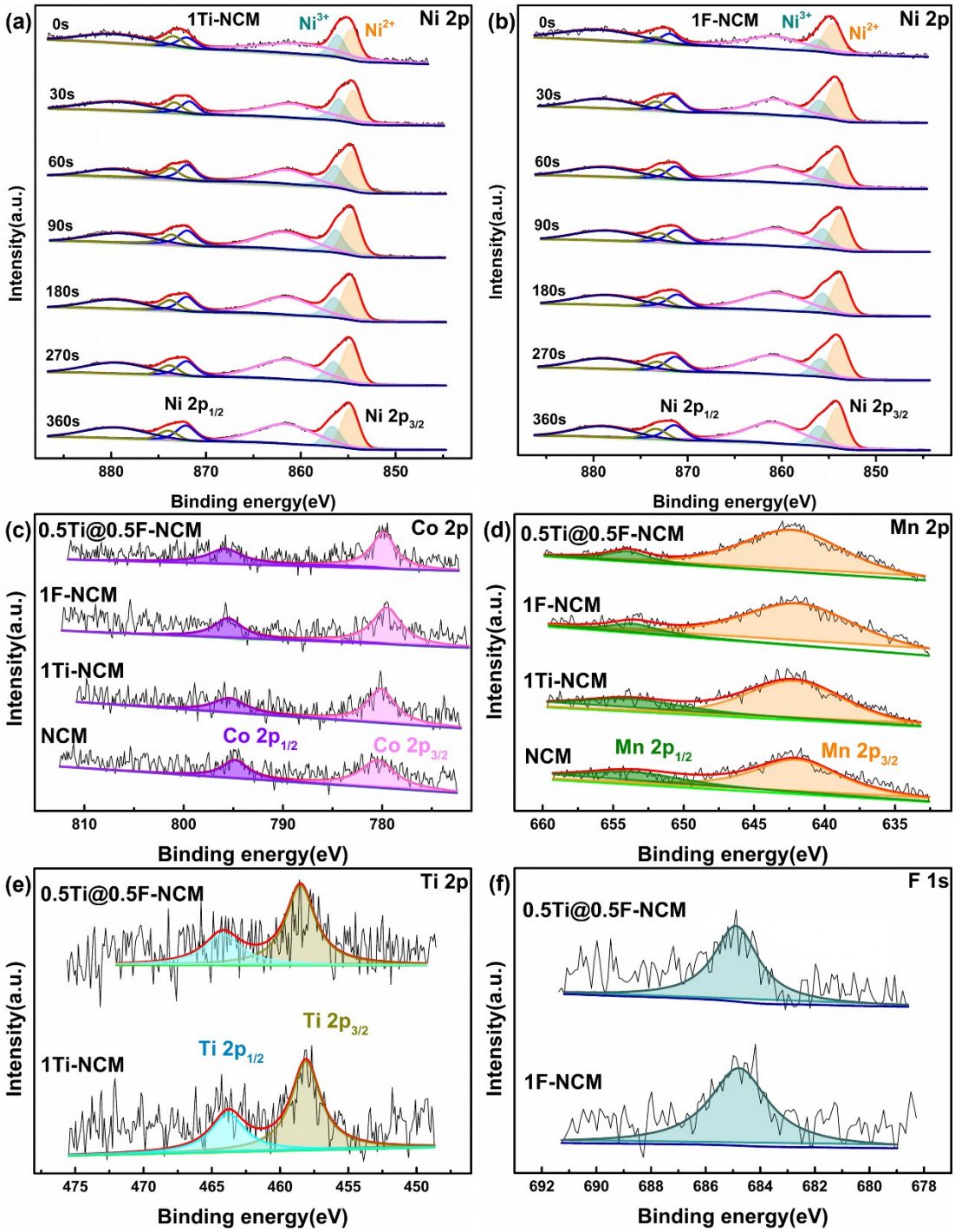

Figure S3. Ni 2p XPS spectra at different etching time for 1F-NCM (a) and 1Ti-NCM (b); XPS spectra of Co 2p(c), Mn 2p(d), Ti 2p(e), F 1s(f) at the etching time of 0 s for NCM, 1Ti-NCM,1F-NCM, and 0.5Ti@0.5F-NCM.

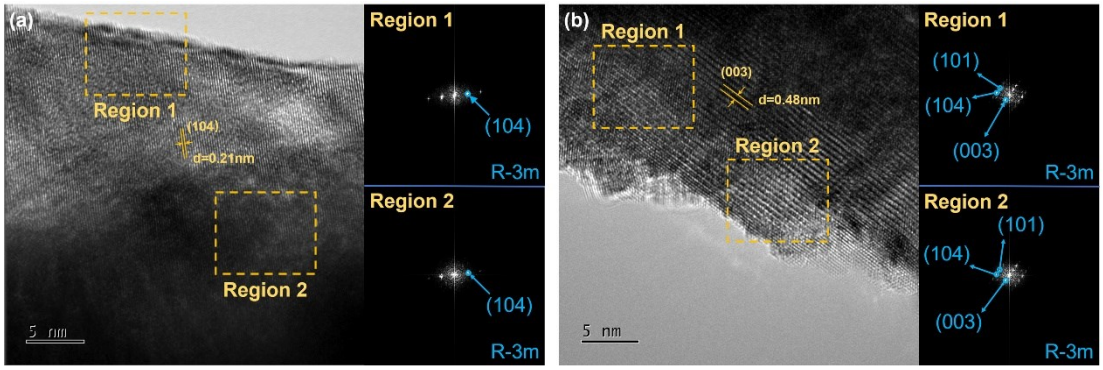

Figure S4. HRTEM images and corresponding FFT patterns for 1Ti-NCM (a) and 1F-NCM (b).

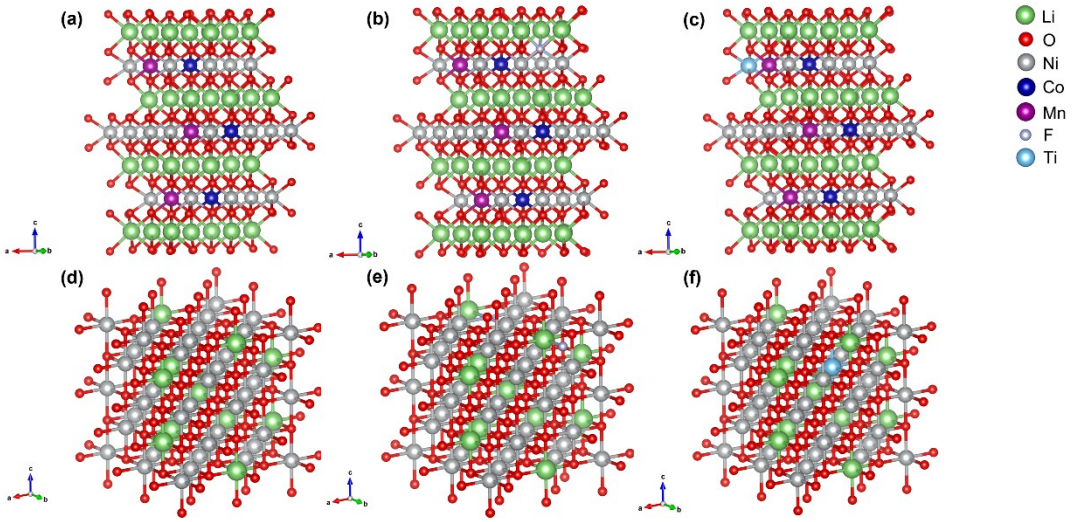

Figure S5. Schematic structures of layered NCM(a), layered F-doped NCM(b), Ti-doped NCM(c), rock-salt phase(d), F-doped rock-salt phase(e) and Ti-doped rock-salt phase(f).

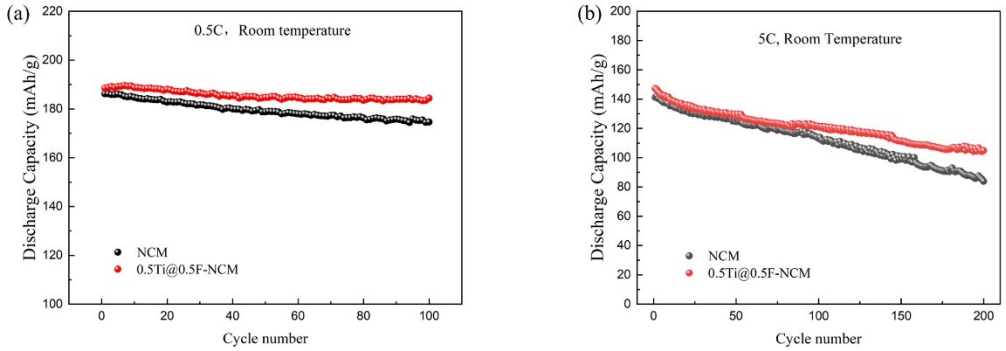

Figure S6. Electrochemical performance (2.8-4.3V) of NCM and 0.5Ti@0.5F-NCM. (a) Long-term cycling performance at 0.5C and room temperature. (b) Long-term cycling performance at 5C and room temperature.

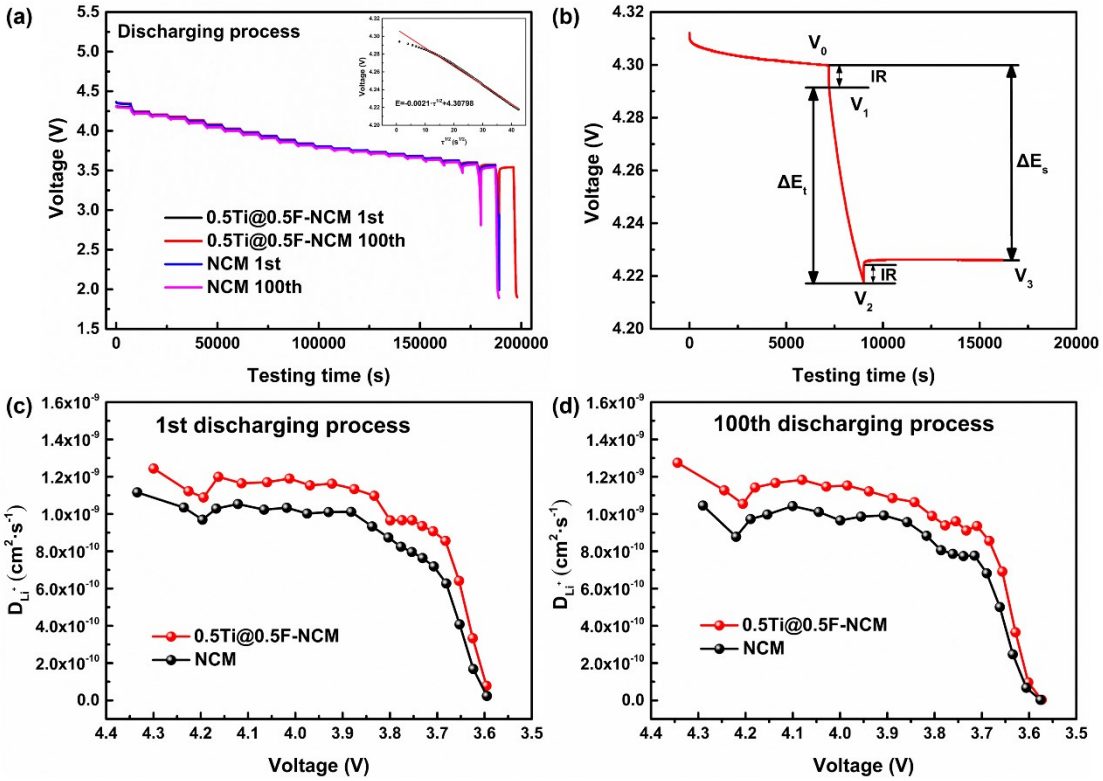

Figure S7. (a) The voltage changes with the testing time in the GITT experiment (insert figure: Linear fit of the cell voltage as a function of the $\tau^{1/2}$); (b) Single titration step of GITT curve for 0.5Ti@0.5F-NCM. The Li-ion diffusion coefficient for NCM and 0.5Ti@0.5F-NCM during the discharging process of (c) the 1st cycle, (d) the 100th cycle.

The GITT experiment was performed on a half-cell. Apply a constant current pulse with a current of 20 mA·g^{-1} for 30 minutes, then let it stand for 2 hours, and repeat this process until the voltage reaches the set value. The diffusion coefficient of Li^+ can be calculated according to the following formula: [1,2]

$$D_{Li^+} = \frac{4}{\pi\tau}\left(\frac{m_B V_M}{M_B S}\right)^2\left(\frac{\Delta E_s}{\Delta E_t}\right)^2 \qquad \left(\tau \ll \frac{L^2}{D_{Li^+}}\right)$$

Where τ is the time of the constant current pulse, S represents the contact area between the cathode active material and the electrolyte, ΔE_t is the voltage change before and after the constant current pulse, and ΔEs is the steady-state voltage change. V_M, M_B and m_B are the molar volume, molar mass and mass of the electrode material, respectively. The value of VM is obtained from the Rietveld refinement results of GSAS. L is the diffusion length.

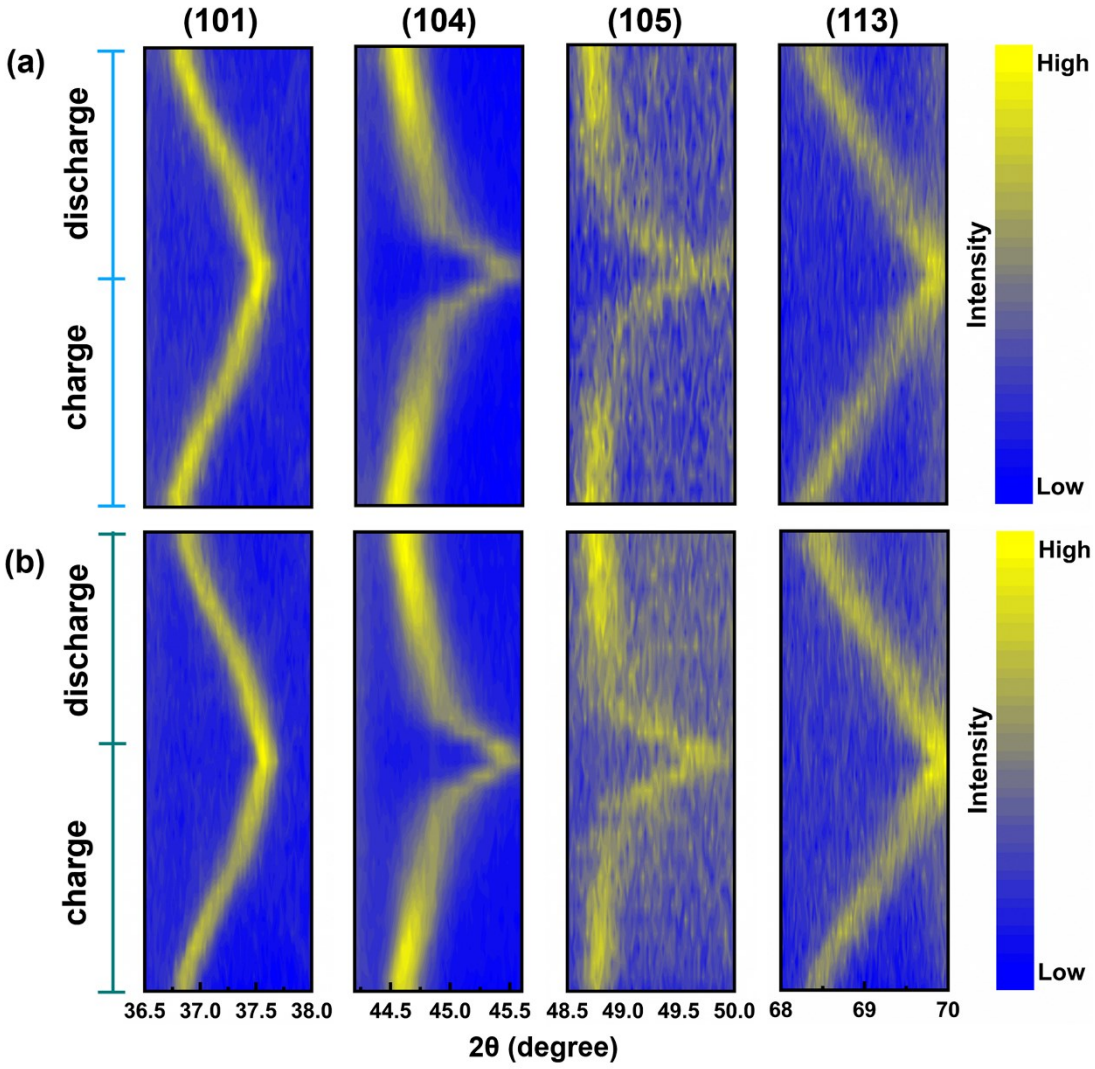

Figure S8. The corresponding contour plots for In-situ XRD tests, (a) NCM and (b) 0.5Ti@0.5F-NCM.

Table S1. Electrochemical performance comparison of Ti/F co-doped Ni-rich cathode with reported modified Ni-rich cathode materials.

Modified method	Voltage range (V)	Current density (mAg^{-1})	Temperature (°C)	Capacity ($mAh\ g^{-1}$)	Retention	Reference
Ti^{4+} doped $LiNi_{0.8}Co_{0.1}Mn_{0.1}O_2$	2.8-4.6	1C=200mAg^{-1}	-	196(0.5C)	84% (1C,100cycles)	3
Ti^{4+} doped $LiNi_{0.8}Co_{0.1}Mn_{0.1}O_2$	2.7-4.3	-	25±2	182.73(0.1C)	89.84% (1C,100cycles)	4
Ti^{4+} doped $LiNi_{0.8}Co_{0.1}Mn_{0.1}O_2$	2.8-4.3	1C=180mAg^{-1}	-	165.60(1C)	77.01% (1C,150cycles)	5
Ti^{4+} and Al^{3+} doped $LiNi_{0.8}Co_{0.1}Mn_{0.1}O_2$	2.7-4.3	1C=180mAg^{-1}	25	189.7(0.1C)	76.75% (1C,200cycles)	6
Ti^{4+} and K^{+} doped $LiNi_{0.8}Co_{0.1}Mn_{0.1}O_2$	2.75-4.35	1C=180mAg^{-1}	25	175.91(1C)	91.19% (1C,200cycles)	7
			55	190.16(1C)	84.38% (1C,100cycles)	
W^{6+} doped $LiNi_{0.8}Co_{0.1}Mn_{0.1}O_2$	2.8-4.5	1C=200mAg^{-1}	27	191.7(1C)	92.1% (1C,100cycles)	8
F^{-} doped $LiNi_{0.8}Co_{0.1}Mn_{0.1}O_2$	2.8-4.3	400 mAg^{-1}	RT	170.1	94.3% (100cycles)	9
F^{-} doped $LiNi_{0.8}Co_{0.1}Mn_{0.1}O_2$	2.8-4.3	100 mAg^{-1}	-	175	93% (150cycles)	10
F^{-} modified $LiNi_{0.8}Co_{0.15}Al_{0.05}O_2$	2.75-4.3	-	-	160(1C)	73% (1C,200cycles)	11
La and F modified $LiNi_{0.8}Co_{0.1}Mn_{0.1}O_2$	2.7-4.3	1C=180mAg^{-1}	25	200.34(0.1C)	90.55% (1C,200cycles)	12
			60	192(1C)	83.28% (1C,150cycles)	
P and F doped $LiNi_{0.8}Co_{0.1}Mn_{0.1}$	3-4.3	1C=170mAg^{-1}	25	199.6(0.1C)	87.6% (1C,100cycles)	13
Li−Nb−O coated and Nb^{5+} doped $LiNi_{0.8}Co_{0.1}Mn_{0.1}O_2$	2.8-4.6	1C=200mAg^{-1}	-	219.1(0.1C)	89.6% (1/3C,60cycles)	14
Zr^{4+} doped $LiNi_{0.8}Co_{0.1}Mn_{0.1}O_2$	2.8-4.3	1C=200mAg^{-1}	-	183.8(0.2C)	84.2% (0.2C,60cycles)	15
Ti^{4+} and F^{-} doped $LiNi_{0.8}Co_{0.1}Mn_{0.1}O_2$	2.8-4.3	1C=200 mAg^{-1}	RT	205.1(0.1C)	93.9% (1C,100cycles)	This work
					89.7% (1C,200cycles)	
					81.4% (1C,300cycles)	
			45	202.2(1C)	94.7% (1C,100cycles)	
					88.1% (1C,200cycles)	

Note: '-'indicates that no information about current density or temperature was found in the reference. 'RT' denotes the room temperature.

Table S2. Binding energy and relative content of Ni^{2+}/Ni^{3+} in Ni 2p XPS spectra for all samples

Sample	Etching times	Ni^{2+}		Ni^{3+}	
		Binding energy (eV)	Relative content (%)	Binding energy (eV)	Relative content (%)
NCM	0s	854.60	52.67	856.10	47.33
	30s	854.39	55.18	856.01	44.82
	60s	854.29	58.55	855.99	41.45
	90s	854.29	67.08	856.17	32.92
	180s	854.35	60.22	856.24	39.78
	270s	854.34	63.90	856.23	36.10
	360s	854.41	65.46	856.31	34.54
0.5Ti@0.5F-NCM	0s	854.85	71.92	856.55	28.08
	30s	854.25	59.41	855.90	40.59
	60s	854.23	60.50	855.94	39.50
	90s	854.17	65.34	855.90	34.66
	180s	854.18	64.42	856.04	35.58
	270s	854.26	65.44	856.09	34.56
	360s	854.28	64.90	856.11	35.10
1F-NCM	0s	854.61	69.71	856.12	30.29
	30s	854.14	67.51	855.97	32.49
	60s	853.96	59.25	855.73	40.75
	90s	853.87	61.30	855.66	38.70
	180s	853.80	61.57	855.65	38.43
	270s	854.00	65.76	855.91	34.24
	360s	854.08	64.28	856.03	35.72
1Ti-NCM	0s	854.71	53.91	856.10	46.09
	30s	854.44	52.73	855.99	47.27
	60s	854.64	55.80	856.34	44.20
	90s	854.66	57.74	856.3	42.26
	180s	854.71	60.38	856.48	39.62
	270s	854.74	65.99	856.53	34.01
	360s	854.80	66.75	856.65	33.25

Table S3. Formation energy of doping for different doping elements in the layered phase

	Formation energy of doping (eV)
F doped NCM	-2.27086496
Ti doped NCM	-6.41273274
Ti@F doped NCM	-8.83634598

Table S4. Formation energy of rock salt phase after different doping elements

	Formation energy (eV)
undoped	-102.7898193
F doped	-104.5824587
Ti doped	-109.3010156
Ti@F doped	-111.1030988

Table S5. Elemental compositions of NCM and the modified samples

Samples	Elemental composition (Atomic %)					
	Ni	Co	Mn	O	Ti	F
NCM	4.49	1.86	2.85	90.8	-	-
1Ti-NCM	9.3	1.7	3.58	84.28	1.13	-
1F-NCM	27.04	3.88	16.37	51.6	-	1.1
0.5Ti@0.5F-NCM	9.44	2.1	6.48	78.44	1.26	2.29

Reference:

1. C. Zhang, J. Wan, Y. Li, S. Zheng, K. Zhou, D. Wang, D. Wang, C. Hong, Z. Gong and Y. Yang, *Journal of Materials Chemistry A*, 2020, **8**, 6893-6901.
2. M. Dong, Z. Wang, H. Li, H. Guo, X. Li, K. Shih and J. Wang, *ACS Sustainable Chemistry & Engineering*, 2017, **5**, 10199-10205.
3. H. Sun, Z. Cao, T. Wang, R. Lin, Y. Li, X. Liu, L. Zhang, F. Lin, Y. Huang and W. Luo, *Materials Today Energy*, 2019, **13**, 145-151.
4. R.-K. Yang, Z.-G. Wu, Y.-C. Li, R. Li, L. Qiu, D. Wang, L. Yang and X.-D. Guo, *Ionics*, 2020, **26**, 3223-3230.
5. D. Zhang, Y. Liu, L. Wu, L. Feng, S. Jin, R. Zhang and M. Jin, *Electrochimica Acta*, 2019, **328**,135086.
6. H. Liu, R. Yang, W. Yang, C. Bai, Y.-C. Li, G. Wang, Y. Liu, W. Xiang, Z. Wu and X. Guo, *Journal of Materials Science*, 2020, **56**, 2347-2359.
7. W. Yao, Y. Liu, D. Li, Q. Zhang, S. Zhong, H. Cheng and Z. Yan, *The Journal of Physical Chemistry C*, 2020, **124**, 2346-2356.
8. G. Shang, Y. Tang, Y. Lai, J. Wu, X. Yang, H. Li, C. Peng, J. Zheng and Z. Zhang, *Journal of Power Sources*, 2019, **423**, 246-254.
9. P. Yue, Z. Wang, H. Guo, X. Xiong and X. Li, *Electrochimica Acta*, 2013, **92**, 1-8.
10. H. Kim, S.-B. Kim, D.-H. Park and K.-W. Park, *Energies*, 2020, **13**,4808.
11. S. Xia, F. Li, F. Cheng, X. Li, C. Sun, J.-J. Liu and G. Hong, *Journal of The Electrochemical Society*, 2018, **165**, A1019-A1026.
12. H. Yang, H. H. Wu, M. Ge, L. Li, Y. Yuan, Q. Yao, J. Chen, L. Xia, J. Zheng, Z. Chen, J. Duan, K. Kisslinger, X. C. Zeng, W. K. Lee, Q. Zhang and J. Lu, *Advanced Functional Materials*, 2019, **29**,1808825.
13. A. Yuan, H. Tang, L. Liu, J. Ying, L. Tan, L. Tan and R. Sun, *Journal of Alloys and Compounds*, 2020, **844**,156210.
14. F. Xin, H. Zhou, X. Chen, M. Zuba, N. Chernova, G. Zhou and M. S. Whittingham, *ACS Appl Mater Interfaces*, 2019, **11**, 34889-34894.
15. S. Gao, X. Zhan and Y.-T. Cheng, *Journal of Power Sources*, 2019, **410-411**, 45-52.